HHS Public Access

Author manuscript

Adv Healthc Mater. Author manuscript; available in PMC 2015 October 22.

Published in final edited form as:

Adv Healthc Mater. 2015 April 22; 4(6): 831–837. doi:10.1002/adhm.201400809.

Collagen Scaffolds Incorporating Coincident Gradations of Instructive Structural and Biochemical Cues for Osteotendinous Junction Engineering

Steven R. Caliari,
Department of Chemical and Biomolecular Engineering, University of Illinois at Urbana-Champaign, 104 RAL, 600 S. Mathews Ave., Urbana, IL 61801, USA

Daniel W. Weisgerber,
Department of Chemical and Biomolecular Engineering, University of Illinois at Urbana-Champaign, 104 RAL, 600 S. Mathews Ave., Urbana, IL 61801, USA

William K. Grier,
Department of Chemical and Biomolecular Engineering, University of Illinois at Urbana-Champaign, 104 RAL, 600 S. Mathews Ave., Urbana, IL 61801, USA

Ziad Mahmassani,
Department of Kinesiology and Community Health, Beckman Institute for Advanced Science and Technology, University of Illinois at Urbana-Champaign, Urbana, IL 61801, USA

Marni D. Boppart, and
Department of Kinesiology and Community Health, Institute for Genomic Biology, Beckman Institute for Advanced Science and Technology, University of Illinois at Urbana-Champaign, Urbana, IL 61801, USA

Prof. Brendan A. C. Harley
Department of Chemical and Biomolecular Engineering, Institute for Genomic Biology, University of Illinois at Urbana-Champaign, 110 RAL, 600 S. Mathews Ave., Urbana, IL 61801, USA

Brendan A. C. Harley: bharley@illinois.edu

Spatially ordered tissues are ubiquitous in the musculoskeletal system and present unique challenges regarding development of biomaterials able to functionally replicate biophysical and biomolecular features of such heterogeneous tissues. While most tissue engineering approaches focus on the repair of single tissues, orthopedic injuries often occur at the interface between soft tissue and bone. Common classes of such multi-tissue junctions include osteochondral (cartilage-bone), meniscus-bone, ligament-bone, and osteotendinous (tendon-bone junction, TBJ) interfaces. A classic example of a commonly injured TBJ is the supraspinatus-humerus junction in the rotator cuff. Notably, the junction contains overlapping patterns of extracellular matrix (ECM) proteins, mineral content, structural alignment, and biochemical signals[1,2] that protect the interface from failure by minimizing

Correspondence to: Brendan A. C. Harley, bharley@illinois.edu.

Supporting Information

Supporting Information is available from the Wiley Online Library or from the author.

stress concentrations.[1–3] Despite the presence of this highly organized junction, it remains a common injury site[1,4] with rotator cuff injuries resulting in over 4 million physician visits and 75 000 surgical procedures per year in the US alone.[5,6] Current clinical approaches forsake biological reintegration for direct mechanical fixation of the tendon to the bone. This approach does not regenerate the graded structure of the interface, with insufficient re-integration responsible for high stress concentrations and resultant high re-failure rates (11%–94%) in some demographics,[3,6,7] highlighting the necessity for improved repair strategies.

The organization of the native osteotendinous interface suggests replicating its spatially ordered properties with biomaterials containing spatially graded interfacial zones may be particularly significant. Further, given the impracticality of obtaining and adequately expanding terminally differentiated osteoblasts and tenocytes, the primary mature cells found across the junction, it is particularly important to develop biomaterials able to drive differentiation of stem cells (i.e., mesenchymal stem cells (MSCs)) down osteotendinous lineages in a spatially selective manner. Such a construct could eventually be seeded with the patient's own MSCs and immediately re-implanted to regenerate the osteotendinous junction. To date, efforts have primarily concentrated on replicating either the spatially graded mineral content[8] or using a combination of structural alignment (anisotropy) and/or mechanical stimulation to drive cell alignment or elicit pro-tenogenic outcomes.[9–11] These data suggest that a biomaterial with spatially graded presentation of tenogenic (geometric anisotropy) and osteogenic (calcium phosphate mineral) cues, in conjunction with mechanical stimulation, may be optimal for TBJ repair.

Here, we report development of an osteotendinous biomaterial based on a collagen-GAG (CG) scaffold platform. CG scaffolds are fabricated by freeze-drying acidic suspensions of collagen and GAG.[12,13] First developed for clinical use as regeneration templates for dermis[12] and peripheral nerve,[14] these scaffolds have more recently been modified for applications in other nonmineralized tissues including cartilage[15] and tendon.[16,17] Calcium phosphate (CGCaP) or hydroxyapatite-mineralized variants have also recently been described for bone applications.[18,19] Our lab has previously described a direction solidification approach to fabricate structurally anisotropic (aligned) CG scaffolds that mimic the native anisotropy of tendon.[17] Notably, the anisotropic scaffold provides contact guidance cues able to encourage 3D alignment and maintenance of tenocyte-specific transcriptomic profiles of equine tenocytes within the matrix.[17,20] We have also described a fabrication approach to integrate disparate nonmineralized and mineralized CG scaffolds into a multi-compartment scaffold for osteochondral applications.[21] In this work, we report an approach to create a collagen scaffold containing coincident gradients of mineralization and geometric anisotropy as seen across the native osteotendinous junction. Further, we demonstrate the spatially gradated scaffold permits spatially selective protenogenic and osteogenic MSC differentiation within a single, 3D biomaterial. Such a biomaterial represents an important enabling technology for MSC-mediated regenerative healing of a range of spatially heterogeneous tissues in the musculoskeletal system.

We first validated the approach of combining directional solidification[17] with suspension layering[21] to create multi-compartment TBJ scaffolds (Figure 1a). Qualitative scanning

electron microscopy (SEM) and quantitative OrientationJ analyses demonstrated that TBJ scaffolds had more aligned pores in the nonmineralized CG compartment while pores were more isotropic in the mineralized CGCaP compartment (Figure 1b,c), mimicking the native TBJ microstructure. Interdiffusion between the two suspension layers was adequate to promote continuity of collagen fibers across the interface (Figure 1g). The creation of a continuous interface was an essential goal of the fabrication process and should improve the ability of the TBJ scaffold to withstand loading without delamination. There are several possible explanations as to why directional solidification induced alignment in the CG but not CGCaP compartment. Given the layering of nonmineralized and mineralized suspensions, it is likely that a balance between conduction-mediated solidification through the copper mold and convection-mediated cooling from the freeze-dryer chamber reduced ice crystal elongation in the mineralized suspension. However, changes in suspension viscosity have previously been shown to affect mass-transfer processes involved in ice crystal coarsening,[17,22] so the increased viscosity of the CGCaP suspension may have contributed to slowing ice crystal aggregation and elongation. Large (>100 μm) pores were observed throughout the TBJ scaffold (Table 1, Supporting Information), a critical design parameter for maintaining cell bioactivity in large, porous constructs.[17,23]

After demonstrating spatially selective control over pore anisotropy within the TBJ scaffold, we confirmed that this fabrication approach was able to maintain regional compartmentalization of mineral content. Micro-computed tomography (micro-CT) shows distinct regions of pixel intensity, indicating the presence of two compositionally distinct compartments (Figure 1e). Identifying the zone defined as having pixel intensities multiple standard deviations outside of those found in each compartment, the scaffold interface was calculated to be 247 ± 101 μm (Figure 1f), a transitional zone similar to the width of native osteotendinous interfaces (100–1000 μm depending on age, species, and tissue interface).[1,11] Finally, to confirm the presence of calcium phosphate mineral, we mapped the distribution of calcium and phosphorus content across the scaffold via energy-dispersive X-ray (EDX) spectroscopy (Figure 1h,i). Superimposing EDX and SEM reveals aligned, nonmineralized scaffold structure merging into a mineralized scaffold compartment with isotropic pores. Previous work with CGCaP scaffolds has characterized the initial phase as brushite, which can be hydrolytically converted to the more biologically relevant hydroxyapatite.[18]

In addition to spatial organization of mineral content and matrix protein organization, the native TBJ also contains distinct profiles of biomolecules, notably multiple members of the transforming growth factor (TGF) superfamily of proteins. Addition of such growth factors has been widely demonstrated within the literature to have beneficial effects for maintaining or driving tenogenic[24] and osteogenic[25] phenotypes. However, media supplementation strategies introduce major concerns, including the need for supraphysiological and/or repeated doses due to diffusive loss. Further, extensive off-label use with BMP-2 for osteogenesis has raised a range of safety concerns.[19] Soluble supplementation also limits the potential for inducing spatially selective responses and can complicate predicting cell response to multiple, competing factors,[26] such as that needed for the osteotendinous interface.

While we have previously demonstrated methods for immobilizing biomolecules within CG scaffolds in a spatially patterned[27] or ubiquitous[28] manner, these methods involved adding factors post-fabrication. In order to enhance the "off-the-shelf" potential of this material, we were interested in directly incorporating biomolecules into the distinct compartments of the TBJ scaffold during fabrication. As a proof of concept, we added fluorescently labeled streptavidin and bovine serum albumin (BSA) into the CG and CGCaP precursor suspensions, prior to layering and freeze-drying ("pre-fabrication" addition). Confocal imaging of the resulting scaffolds revealed selective incorporation and compartmentalization of the disparate proteins across the scaffold (Figure 2a). Importantly, no difference ($p = 0.42$) in loading efficiency was observed between prefabrication (added directly to the suspension immediately before freeze-drying) or post-fabrication (incorporated via conventional carbodiimide cross-linking to scaffolds) addition of fluorescently labeled BSA or bone morphogenetic protein (BMP) (Figure 2b). Additionally, biological activity of the proteins was maintained through the freeze-drying process as demonstrated by incorporation of the mitogenic factor platelet-derived growth factor-BB (PDGF-BB) into the scaffold. Equivalent amounts of PDGF-BB (400 ng per scaffold) added pre- and post-fabrication both led to significantly ($p < 0.02$) increased MSC metabolic activity after 7 d culture compared to a nonsup-plemented control, with no difference between pre- or post-fabrication addition ($p = 0.89$) (Figure 2c).

After determining the microstructural and compositional properties of the TBJ scaffold, we examined the combined impact of a spatially graded scaffold and uniaxial tensile stimulation on MSC bioactivity. For this work, we adapted a stretch paradigm based on Paxton et al., which optimized stretch conditions in an engineered fibrin gel system for ligament tissue engineering to maximize collagen synthesis and mechanical integrity (Figure 3a).[10] The bioreactor used was a commercially available Flexcell system that has been applied to stimulate a range of biomaterial substrates.[29] We were also interested in identifying differences in how MSCs sensed their local microenvironment across the scaffold as a function of load, and examined fibronectin-related integrin subunits $\alpha 4$, $\alpha 5$, αV, $\beta 1$, and $\beta 3$, known to impact MSC proliferation and differentiation.[30] Fibronectin-associated integrin expression has been shown to be dependent on mechanical stretch for a variety of cell types, including fibroblasts[31] and MSCs.[32] Our results indicate that MSCs attach and spread throughout the TBJ scaffold in response to disparate contact guidance cues provided across the scaffold (Figure 3b). MSCs in the nonmineralized tendinous compartment consistently express fibronectin-related integrins at a higher level than in the mineralized osseous compartment as early as 24 h post-seeding, with $\beta 1$ subunit expression significantly ($p = 0.04$) higher in the tendinous compartment (Figure 3c,d). MSCs in both compartments trended towards increased integrin expression in response to stretch (Figure 3d). These trends are also consistent with previous work that showed integrin–ECM complexes are more easily disrupted on softer substrates, such as the nonmineralized CG versus mineralized CGCaP scaffold compartment,[33] leading to increased overall integrin expression.[34]

We subsequently examined whether the combination of intermittent stretch and the spatially graded TBJ scaffold could lead to spatially graded MSC specification down osteotendinous

lineages during a 6-week culture period. Metabolic activity of MSCs increased over the culture period (Figure 1, Supporting Information). Although MSCs in static culture showed significantly ($p = 0.02$) greater metabolic activity after 4 weeks than MSCs under dynamic stretch, the stretch group showed significant ($p = 0.002$) increases in metabolic activity from week 4 to 6 so that by the conclusion of the study there were no significant differences between groups ($p = 0.23$).

Expression levels of pro-osteogenic genes (*ALP*, *BSP*, and *OCN*) and pro-tenogenic genes (*COL1A1*, *SCXB*, and *TNC*) were assessed for MSCs isolated from tendinous and osseous compartments of TBJ scaffolds after 6 weeks culture in growth media. Notably, *BSP* and *OCN* were both significantly ($p < 0.05$) upregulated in the mineralized osseous compartment compared to the nonmineralized tendinous compartment (Figure 4a, Figure 2a, Supporting Information). Examining markers of tenogenesis within the tendinous compartment, dynamic stretch induced an increase in scleraxis (*SCXB*) expression as well as a significant ($p = 0.04$) upregulation of the *COL1A1* gene (Figure 4b, Figure 2b, Supporting Information). Generally, stretch led to decreased expression of osteogenic markers but increased expression of tenogenic markers in both scaffold compartments (Figure 4, Figure 2, Supporting Information). These findings are consistent with recent observations from our laboratory regarding selective structural modifications to the CG scaffold to support tenogenic versus osteogenic phenotypes in monolithic scaffolds.[35] However, here we demonstrate induction of divergent lineage selection across a single 3D scaffold maintained in conventional growth media without addition of biomolecular factors (e.g., GDF, BMP)[36] to augment cell response.

Scaffold structural organization and remodeling after 6 weeks of culture was evaluated via histology and confocal imaging. H&E analyses revealed cell infiltration in both tendinous and osseous scaffold compartments with no discernible differences as a result of applied stretch (Figure 4c,d). This was expected as the freezing temperature during fabrication (−10 °C) was chosen to generate larger pores (>150 μm) that facilitate cell migration, biotransport, and subsequent cell metabolic activity,[17] and greater resistance to cell-mediated contractile forces.[17] Collagen organization was measured using SHG imaging, revealing more organized, aligned collagen fibers in the tendinous compartment compared to the osseous compartment (Figure 3, Supporting Information). Quantification of collagen fiber alignment indicated that while stretch and presence of MSCs within the matrix over 6 weeks does not seem to affect collagen alignment within each compartment, there is an overall trend towards increased alignment and organization in the tendinous compartment that persists (Figure 3c, Supporting Information). An important limitation of SHG when used in conjunction with collagen-based materials is that there is no way to differentiate between scaffold and cell-synthesized collagen. However, given the aligned CG scaffold is known to provide critical contact guidance cues to induce and maintain cell alignment,[20] the maintenance of an aligned phenotype across 6 week culture suggests the osteotendinous scaffold supports cell-mediated remodeling of an aligned microstructure. Similarly, restriction of mineral content as assessed by alizarin red staining to the osseous compartment (Figure 4e,f), coupled with our previous observation that up to 80% of the mineral content from the mineralized CGCaP scaffold dissolves over 6 weeks in vitro[37] suggests

significant new mineral formation and matrix remodeling is taking place. Maintenance of a discrete mineralization front suggests that limited mineral deposition was taking place within the tendinous CG compartment, consistent with our observation of divergent osteotendinous lineage specification.

Together these data show that the multi-compartment TBJ scaffold introduced here can mimic key microstructural and compositional characteristics of the native TBJ, and that in conjunction with uniaxial tensile strain can guide spatially selective MSC differentiation down osteotendinous interface specific lineages. Notably, this material is the first 3D scaffold to display coincident gradients of structural alignment, mineral content, and biomolecule presentation as seen across the native osteotendinous junction. Further, this study integrates biomaterial-based approaches optimized for pro-tenogenic (e.g., pore/fiber alignment) or osteogenic (e.g., mineral content) MSC differentiation into a single-graded material for the first time. Moving forward, ongoing efforts are optimizing stimulation profiles and tracing compartment-specific strain profiles in order to identify loading strategies to balance cell attachment, proliferation, and phenotypic changes. Ongoing in vivo studies will begin to ascertain the suitability of these materials for TBJ repair, and are taking advantage of recently described approaches to mechanically reinforce these CG scaffolds using a core–shell composite design strategy[16,38] that does not impact the scaffold design reported here.

Experimental Section

Complete procedures can be found in the Supporting Information. All materials were purchased from Sigma-Aldrich (St Louis, MO) unless otherwise specified.

Scaffold Fabrication via Freeze-Drying

TBJ scaffolds were fabricated by combining directional solidification[17] with a liquid-phase co-synthesis method[21] (Figure 1). A thermally mismatched mold composed of a Teflon body joined to a 1/16″ thick copper base was used for the freeze-drying process to induce directional solidification. First, degassed CG suspension was pipetted into cylindrical holes in the Teflon-copper mold (6 mm diameter, 15 mm deep). The CGCaP suspension was carefully layered on top of the CG suspension (CG:CGCaP suspension volume ratio 2:1). The suspensions were allowed to interdiffuse at 4 °C for 20 min prior to freeze-drying. For biomolecule incorporation, AlexaFluor 488-streptavidin conjugate (Invitrogen) and AlexaFluor 594-BSA conjugate (Invitrogen) were directly added to the degassed CGCaP and CG suspensions, respectively, at a final concentration of 1 μg mL^{-1} immediately prior freeze-drying. The suspension-loaded mold was placed on a freeze-dryer shelf (VirTis) precooled to −10 °C and maintained at this temperature for 2 h to complete freezing. Following freezing, the shelf temperature was ramped up to 0 °C at a rate of 1 °C min^{-1} while pulling a vacuum of 200 mTorr to remove ice crystals via sublimation. Freeze-drying results in the formation of dry, macroporous scaffolds that are amenable to post-fabrication hydration, cross-linking, and cell seeding.[13,17,21]

SEM and EDX Analyses

Scanning electron microscopy and energy-dispersive X-ray spectroscopy were used to qualitatively assess scaffold microarchitecture and elemental composition, respectively. SEM/EDX analyses were executed on a JEOL JSM-6060LV low-vacuum scanning electron microscope (JEOL USA) using a combination of secondary and backscatter electron detection under low vacuum to enable scaffold visualization without a conductive coating.[21] EDX compositional mapping data were gathered for calcium (Ca) and phosphorus (P) content across longitudinal interfacial sections of the multi-compartment scaffolds.

Micro-CT Analysis

Micro-computed tomography analysis was performed with Xradia Micro-XCT-400 at 25 kEv and 5 W. Total scaffold scans were performed with a voxel size of 15 μm; scans to determine width of the interface between CG and CGCaP compartments used a voxel size of 4 μm. Interface width was determined by projecting a 4 × 4 grid of squares (individual square size: 670 μm × 670 μm) through the height of the scaffold. The average pixel intensity of each data point (square) in the Z-stack was then calculated. Z-slices possessing an average intensity between the mean ± 3 StDev of the first image slice (pure CGCaP) and the last image slice (pure CG) were considered part of the interfacial region.[39]

Quantitative Assessment of Scaffold strut and Collagen Fiber Alignment

Scaffold strut alignment was quantified using the OrientationJ plugin within ImageJ.[40] SEM images (30× magnification) of both the transverse and longitudinal planes in the CG and CGCaP compartments were used for the analysis. Scaffold strut alignment was quantified using OrientationJ's "Distribution" function. Alignment of collagen fibers was quantified from confocal images acquired through SHG imaging. Orientation angles of individual collagen fibers (100 per group) were measured using the 'Measure' function. Alignment data were reported in terms of orientation angle (−90° to +90°) where 0° corresponds to direction of heat transfer during freezing in the longitudinal plane.

Supplementary Material

Refer to Web version on PubMed Central for supplementary material.

Acknowledgments

The authors acknowledge Donna Epps (IGB, UIUC) for assistance with histology, Dr. Mayandi Sivagura (IGB, UIUC) for assistance with confocal microscopy, Dr. Sandra McMasters (SCS, UIUC) for preparation of culture media, and the IGB Core Facilities for assistance with real-time PCR. This material is based upon work supported by the National Science Foundation under Grant No. 1105300. Research reported in this publication was supported by the National Institute of Arthritis and Musculoskeletal and Skin Diseases of the National Institutes of Health under Award Numbers R21 AR063331. D.W.W. was funded at UIUC from National Science Foundation Grant 0965918 IGERT: Training the Next Generation of Researchers in Cellular & Molecular Mechanics and BioNanotechnology. The authors are grateful for the funding for this study provided by the Chemistry-Biology Interface Training Program NIH NIGMS T32GM070421 (SRC, WKG), the Chemical and Biomolecular Engineering Dept. (BAH), and the Institute for Genomic Biology (BAH) at the University of Illinois at Urbana-Champaign. This research was carried out in part in the Frederick Seitz Materials Research Laboratory Central Facilities, University of Illinois, which are partially supported by the US Department of Energy under grants DE-FG02–07ER46453 and DE-FG02–07ER46471.

References

1. Wopenka B, Kent A, Pasteris JD, Yoon Y, Thomopoulos S. Appl Spectrosc. 2008; 62:1285. [PubMed: 19094386]
2. a) Thomopoulos S, Genin GM, Galatz LM. J Musculoskelet Neuronal Interact. 2010; 10:35. [PubMed: 20190378] b) Genin GM, Kent A, Birman V, Wopenka B, Pasteris JD, Marquez PJ, Thomopoulos S. Biophys J. 2009; 97:976. [PubMed: 19686644]
3. Galatz L, Rothermich S, VanderPloeg K, Petersen B, Sandell L, Thomopoulos S. J Orthop Res. 2007; 25:1621. [PubMed: 17600822]
4. Woo SL, Debski RE, Zeminski J, Abramowitch SD, Saw SS, Fenwick JA. Annu Rev Biomed Eng. 2000; 2:83. [PubMed: 11701508]
5. Vitale MA, Vitale MG, Zivin JG, Braman JP, Bigliani LU, Flatow EL. J Shoulder Elbow Surg. 2007; 16:181. [PubMed: 17399623]
6. Butler DL, Juncosa-Melvin N, Boivin GP, Galloway MT, Shearn JT, Gooch C, Awad H. J Orthop Res. 2008; 26:1. [PubMed: 17676628]
7. Klepps S, Bishop J, Lin J, Cahlon O, Strauss A, Hayes P, Flatow EL. Am J Sports Med. 2004; 32:1716. [PubMed: 15494338]
8. a) Phillips JE, Burns KL, Le Doux JM, Guldberg RE, Garcia AJ. Proc Natl Acad Sci USA. 2008; 105:12170. [PubMed: 18719120] b) Mutsuzaki H, Sakane M, Fujie H, Hattori S, Kobayashi H, Ochiai N. Am J Sports Med. 2011; 39:1059. [PubMed: 21220545] c) Samavedi S, Guelcher SA, Goldstein AS, Whittington AR. Biomaterials. 2012; 33:7727. [PubMed: 22835644] d) Li X, Xie J, Lipner J, Yuan X, Thomopoulos S, Xia Y. Nano Lett. 2009; 9:2763. [PubMed: 19537737]
9. a) Moffat KL, Kwei AS, Spalazzi JP, Doty SB, Levine WN, Lu HH. Tissue Eng Part A. 2009; 15:115. [PubMed: 18788982] b) Subramony SD, Dargis BR, Castillo M, Azeloglu EU, Tracey MS, Su A, Lu HH. Biomaterials. 2013; 34:1942. [PubMed: 23245926]
10. Paxton JZ, Hagerty P, Andrick JJ, Baar K. Tissue Eng Pt A. 2012; 18:277.
11. Moffat KL, Sun WH, Pena PE, Chahine NO, Doty SB, Ateshian GA, Hung CT, Lu HH. Proc Natl Acad Sci USA. 2008; 105:7947. [PubMed: 18541916]
12. Yannas IV, Lee E, Orgill DP, Skrabut EM, Murphy GF. Proc Natl Acad Sci USA. 1989; 86:933. [PubMed: 2915988]
13. O'Brien FJ, Harley BA, Yannas IV, Gibson L. Biomaterials. 2004; 25:1077. [PubMed: 14615173]
14. Chamberlain LJ, Yannas IV, Hsu HP, Strichartz GR, Spector M. J Neurosci Res. 2000; 60:666. [PubMed: 10820438]
15. a) Vickers SM, Gotterbarm T, Spector M. J Orthop Res. 2010; 28:1184. [PubMed: 20225321] b) Capito RM, Spector M. Gene Ther. 2007; 14:721. [PubMed: 17315042]
16. Caliari SR, Ramirez MA, Harley BAC. Biomaterials. 2011; 32:8990. [PubMed: 21880362]
17. Caliari SR, Harley BAC. Biomaterials. 2011; 32:5330. [PubMed: 21550653]
18. Harley BA, Lynn AK, Wissner-Gross Z, Bonfield W, Yannas IV, Gibson LJ. J Biomed Mater Res A. 2010; 92:1066. [PubMed: 19301274]
19. Lyons FG, Gleeson JP, Partap S, Coghlan K, O'Brien FJ. Clin Orthop Relat Res. 2014; 472:1318. [PubMed: 24385037]
20. Caliari SR, Weisgerber DW, Ramirez MA, Kelkhoff DO, Harley BAC. J Mech Behav Biomed Mater. 2012; 11:27. [PubMed: 22658152]
21. Harley BA, Lynn AK, Wissner-Gross Z, Bonfield W, Yannas IV, Gibson LJ. J Biomed Mater Res A. 2010; 92:1078. [PubMed: 19301263]
22. Haugh MG, Murphy CM, O'Brien FJ. Tissue Eng Part C Methods. 2010; 16:887. [PubMed: 19903089]
23. O'Brien FJ, Harley BA, Waller MA, Yannas IV, Gibson LJ, Prendergast PJ. Technol HealthCare. 2007; 15:3.
24. a) Thomopoulos S, Harwood FL, Silva MJ, Amiel D, Gelberman RH. J Hand Surg Am. 2005; 30A:441. [PubMed: 15925149] b) Park A, Hogan MV, Kesturu GS, James R, Balian G, Chhabra AB. Tissue Eng Part A. 2010; 16:2941. [PubMed: 20575691] c) Manning CN, Kim HM,

Sakiyama-Elbert S, Galatz LM, Havlioglu N, Thomopoulos S. J Orthop Res. 2011; 29:1099. [PubMed: 21246611]

25. a) Yilgor P, Tuzlakoglu K, Reis RL, Hasirci N, Hasirci V. Biomaterials. 2009; 30:3551. [PubMed: 19361857] b) Lan Levengood SK, Polak SJ, Poellmann MJ, Hoelzle DJ, Maki AJ, Clark SG, Wheeler MB, Wagoner Johnson AJ. Acta Biomater. 2010; 6:3283. [PubMed: 20176148]
26. a) Caliari SR, Harley BA. Tissue Eng Part A. 2014; 20:2463. [PubMed: 24568607] b) Khetan S, Guvendiren M, Legant WR, Cohen DM, Chen CS, Burdick JA. Nat Mater. 2013; 12:458. [PubMed: 23524375]
27. Martin TA, Caliari SR, Williford PD, Harley BA, Bailey RC. Biomaterials. 2011; 32:3949. [PubMed: 21397322]
28. Caliari SR, Harley BA. Tissue Eng Part A. 2013; 19:1100. [PubMed: 23157454]
29. a) Ahearne M, Bagnaninchi PO, Yang Y, El Haj AJ. J Tissue Eng Regen Med. 2008; 2:521. [PubMed: 18956413] b) Boerboom RA, Rubbens MP, Driessen NJ, Bouten CV, Baaijens FP. Ann Biomed Eng. 2008; 36:244. [PubMed: 18066665]
30. Allen JL, Cooke ME, Alliston T. Mol Biol Cell. 2012; 23:3731. [PubMed: 22833566]
31. Steward RL Jr, Cheng CM, Ye JD, Bellin RM, LeDuc PR. Sci Rep. 2011; 1:147. [PubMed: 22355663]
32. Kinneberg KR, Nirmalanandhan VS, Juncosa-Melvin N, Powell HM, Boyce ST, Shearn JT, Butler DL. J Orthop Res. 2010; 28:1092. [PubMed: 20143407]
33. Weisgerber DW, Kelkhoff DO, Caliari SR, Harley BAC. J Mech Behav Biomed Mater. 2013; 28:26. [PubMed: 23973610]
34. Du J, Chen XF, Liang XD, Zhang GY, Xu J, He LR, Zhan QY, Feng XQ, Chien S, Yang C. Proc Natl Acad Sci USA. 2011; 108:9466. [PubMed: 21593411]
35. Caliari SR, Harley BAC. Adv Healthcare Mater. 2014; 3:1086.
36. Ker EDF, Chu B, Phillippi JA, Gharaibeh B, Huard J, Weiss LE, Campbell PG. Biomaterials. 2011; 32:3413. [PubMed: 21316755]
37. Weisgerber DW, Caliari SR, CHarley BA. Biomater Sci. 201510.1039/c4bm00397g
38. Caliari SR, Mozdzen LC, Armitage O, Oyen ML, Harley BAC. J Biomed Mater Res Part A. 2014; 102:917.
39. Weisgerber DW, Kelkhoff DO, Caliari SR, Harley BA. J Mech Behav Biomed Mater. 2013; 28C: 26. [PubMed: 23973610]
40. Fonck E, Feigl GG, Fasel J, Sage D, Unser M, Rufenacht DA, Stergiopulos N. Stroke. 2009; 40:2552. [PubMed: 19478233]

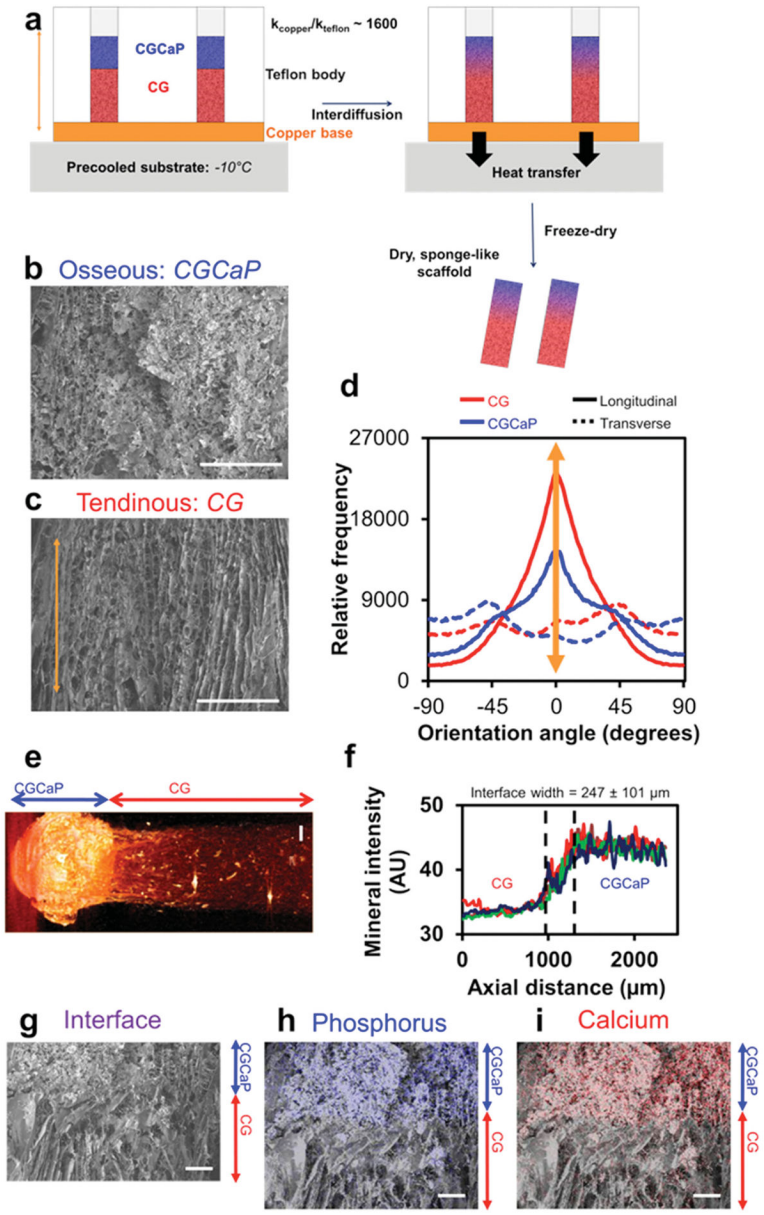

Figure 1.

Microarchitecture and calcium phosphate content of multi-compartment TBJ scaffolds. a) Schematic of approach to make multicompartment osteotendinous scaffolds with distinct regions of pore anisotropy and mineral content. The approach combined directional solidification to produce aligned pores with liquid phase co-synthesis to integrate the nonmineralized CG (red) and mineralized CGCaP (blue) compartments together into a single construct. Scanning electron micrographs indicate b) relatively isotropic pores in the mineralized osseous (CGCaP) region and c) highly aligned pores in the non-mineralized tendinous (CG) region. Scale bars: 200 μm. d) OrientationJ analysis of pore alignment demonstrated that pores were longitudinally aligned in the tendinous compartment, but more randomly aligned in the corresponding osseous compartment. e) Micro-CT image of osteotendinous scaffold. Scale bar: 1 mm. f) Using differences in the intensity of the

mineralized versus nonmineralized compartments, the interface width was calculated to be approximately 247 ± 101 μm. g) continuity of collagen fibers at the interface between compartments was demonstrated with energy-dispersive X-ray spectroscopy analysis revealing localization of h) calcium and i) phosphorus content primarily in the mineralized osseous region of the scaffold. Scale bars: 200 μm.

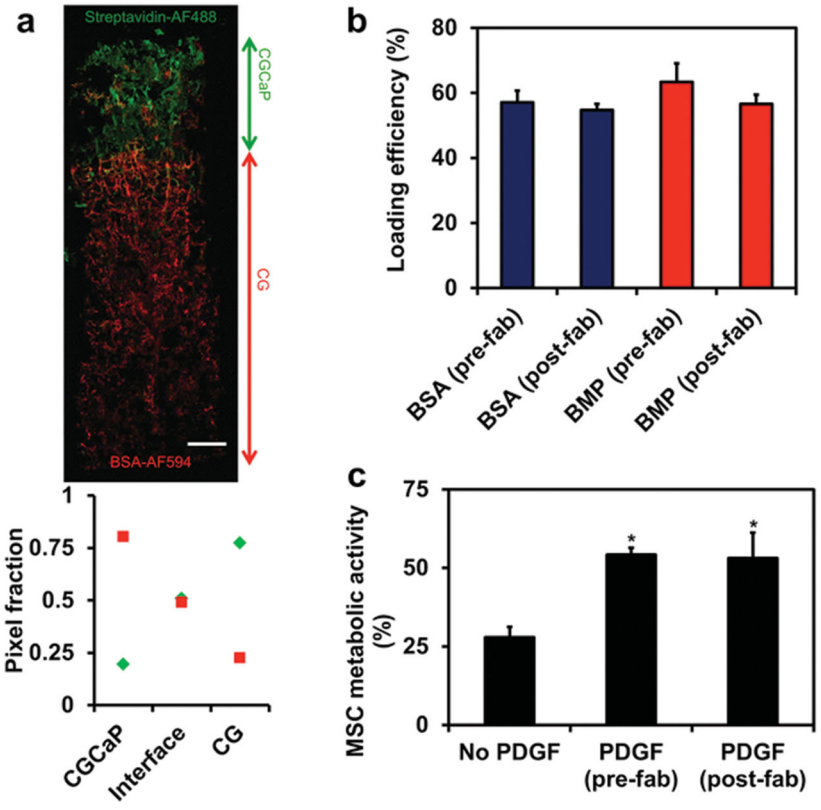

Figure 2.

Direct incorporation of biomolecules across the osteotendinous scaffolds during lyophilization. a) Confocal micrograph of osteotendinous scaffold loaded with AlexaFluor 488-streptavidin conjugate in the mineralized (CGCaP) compartment and AlexaFluor 594-BSA conjugate in the non-mineralized (CG) compartment. b) Loading efficiency of fluorescently-labeled BSA and BMP-2 when added in equivalent amount either pre-fabrication (during lyophilization) or post-fabrication (via carbodiimide cross-linking). c) MSC metabolic activity on scaffolds with no PDGF or PDGF incorporated either pre- or post-fabrication. Scale bar: 1 mm. *: significantly higher than the no PDGF group.

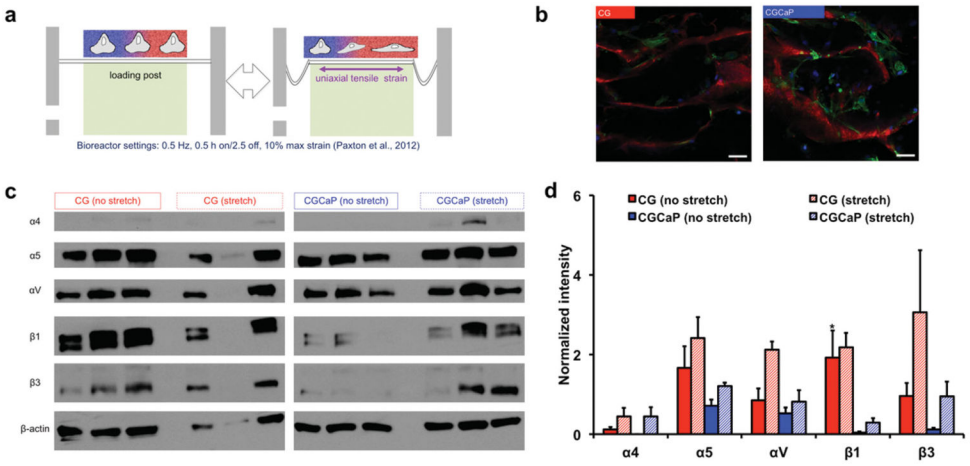

Figure 3.

Influence of local scaffold microenvironment and applied tensile load on integrin expression profiles. a) Schematic of Flexcell bioreactor system loaded with MSC-seeded osteotendinous scaffold. b) Representative confocal micrographs of MSCs within distinct tendinous and osseous compartments. Green channel: actin, Red channel: collagen scaffold, Blue channel: nuclei, Scale bars: 50 μm. c) Western blots of fibronectin-related integrin subunit expression profiles in tendinous and osseous compartments under static and dynamic culture, showing consistently higher expression in the tendinous compartment and in response to stretch. d) Normalized blot intensity quantitatively showed higher levels of expression in the tendinous compartment and in response to tensile loading across both compartments. *: significantly higher expression than CGCaP compartment.

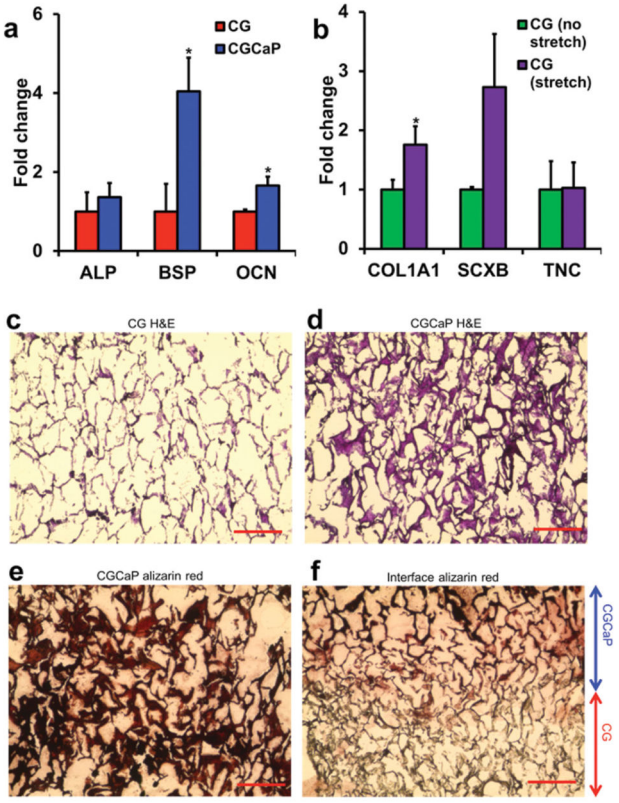

Figure 4.

MSC gene expression and histology after 6-week culture period. a) Expression of osteogenic genes alkaline phosphatase (*ALP*), bone sialoprotein (*BSP*), and osteocalcin (*OCN*) was elevated in the mineralized osseous compartment. b) Expression of tenogenic markers type I collagen (*COL1A1*), scleraxis (*SCXB*), and tenascin-C (*TNC*) was elevated in the tendinous compartment in response to tensile stimulation. Hema-toxylin and eosin (H&E) staining of the c) tendinous and d) osseous compartments revealed MSC infiltration throughout the scaffold. e) Mineral staining via alizarin red showed mineral localized primarily to the osseous compartment and f) not in the tendinous compartment. *: significantly higher expression. Scale bars: 200 μm.